

2024

Numerical Study on Enhancing the Geotechnical Behavior of Strip Footings on Oil-Contaminated Sand Using Stone Columns

Ahmad Nasr

Tanta University - Faculty of Engineering, ahmed.nasr@f-eng.tanta.edu.eg

Waseim Azzam

Tanta University - Faculty of Engineering, azzam_waseim@yahoo.com

Mohamed Ahmed Mahmoud Abdelrehem

Tanta University - Faculty of Engineering, mabdelraheem890@gmail.com

Follow this and additional works at: <https://digitalcommons.aaru.edu.jo/erjeng>



Part of the [Civil Engineering Commons](#), and the [Geotechnical Engineering Commons](#)

Recommended Citation

Nasr, Ahmad; Azzam, Waseim; and Mahmoud, Mohamed Ahmed Abdelrehem (2024) "Numerical Study on Enhancing the Geotechnical Behavior of Strip Footings on Oil-Contaminated Sand Using Stone Columns," *Journal of Engineering Research*: Vol. 8: Iss. 4, Article 15.

Available at: <https://digitalcommons.aaru.edu.jo/erjeng/vol8/iss4/15>

This Article is brought to you for free and open access by Arab Journals Platform. It has been accepted for inclusion in Journal of Engineering Research by an authorized editor. The journal is hosted on [Digital Commons](#), an Elsevier platform. For more information, please contact marah@aarj.edu.jo, rakan@aarj.edu.jo.

Numerical Study on Enhancing the Geotechnical Behavior of Strip Footings on Oil-Contaminated Sand Using Stone Columns

Nasr, A. M¹, Azzam, W. R² and Mahmoud, M. A³

¹ Professor, Structural Engineering Department, Tanta University, Egypt

² Professor, Structural Engineering Department, Tanta University, Egypt

³ M. Sc. Research Student, Structural Engineering Department, Tanta University, Egypt

*Corresponding author: Mohammad146552@f-eng.tanta.edu.eg

Abstract: Ground improvement techniques are frequently employed in construction sites characterized by weak soil conditions that may result in suboptimal performance. The use of ordinary and encased stone columns aims to enhance endurance, shear strength, and soil hardness, thereby mitigating settlement issues and expediting the consolidation of contaminated sand soils. In this research, a comprehensive investigation involving 74 cases was conducted to assess the behavior of both ordinary stone columns and encased stone columns under strip footing in contaminated sand subgrade. The objective was to discern the impact and characteristics of encapsulation in comparison to encapsulated stone columns, employing a Finite Element Model (FEM) within the PLAXIS 3D software package. The study focused on stone columns with two different diameters ($D = 0.5$ m and 0.6 m), while the column length was 12m across all cases. As the contamination level increases - at the variable contaminated sand levels of (2%, 5%, and 10%) - the viscosity of the soil rises, leading to a reduction in cohesion between soil granules. Consequently, the internal friction angle decreases, with values diminishing from 31° to 27° and then to 24° , respectively. The clean sand was placed to achieve relative density, a medium dense sand state ($D_r = 50\%$). The two categories of stone columns examined were ordinary stone columns (OSC) without encapsulation and encased stone columns (ESC) encapsulated with varying degrees of hardening. Results obtained at variable

internal friction angles (35, 40, and 45 degrees) revealed a notable increase in the endurance of ordinary stone columns on untreated soil conditions, reaching 100%, 125%, and 148% for column diameters ($D = 0.5$ m) and 130%, 145%, and 180% for column diameters ($D = 0.6$ m), respectively. The corresponding increase in the endurance of encased stone columns under untreated soil conditions was found to be 275%, 33%, and 345% for column diameters ($D = 0.5$ m) and reached 313%, 350%, and 375% for column diameters ($D = 0.6$ m), respectively. All preceding results were obtained under the condition of a contaminated sand content of 5%. The investigation aimed to provide valuable insights into the performance and efficacy of ordinary stone columns (OSC) and encased stone columns (ESC) as a geotechnical solution for improving soil conditions in construction projects.

Keywords: Clean sand; Contaminated sand; Ordinary Stone Columns; Encased stone columns; PLAXIS 3D; Applied load; Settlement.

INTRODUCTION

One of the pivotal methods for ground improvement using stone columns involves employing geosynthetic reinforcement, which reduces horizontal drainage paths, enhances shear strength, reduces settlement, and accelerates consolidation in cohesive soils. Stone columns aim to increase bearing capacity,

reduce settlement, and mitigate liquefaction potential, surpassing alternatives like replacement methods due to their advantages, including high friction angle, stiffness, and pore pressure dissipation. Stone columns can withstand heavier loads and induce fewer settlements compared to untreated soil, even mitigating liquefaction in loose sand. The main target of a stone column is to increase the bearing capacity, decrease settlement, and decrease liquefaction potential. The alternative solution of using the replacement method is also eliminated because of dewatering, groundwater monitoring, and groundwater cut-off. The granular material has a lot of advantages over other filling materials because of its high friction angle, stiffness, and dissipation of pore pressure. Datye (1982) reported that the granular columns are more economical than the vertical drains. Van Impe and Silence (1986) used geosynthetic material to encase granular columns. Van Impe et al. (1997) reported that stone columns can carry higher loads and induce smaller settlements compared with untreated soil. In addition, these columns can minimize the liquefaction effect in loose sand. Han and Yee (2001) reported that granular columns decrease consolidation time over vertical drains due to the diameter ratio and the stress concentration ratio. The stress applied is redistributed to the column and the surrounding soil during consolidation time. The ratio of stress on the column to the stress on the soil is defined as the stress concentration ratio. The diameter ratio of stone columns ranges from 1.5 to 5, but the diameter ratio range of vertical drains ranges from 5 to 100. The authors report that a negligible increase in the bearing capacity of stone columns is gained by increasing column length beyond 6 d. However, the undrained stiffness of footings is observed to increase for columns longer than 6d, which suggests that there are some merits in installing columns longer than this critical length for settlement control. The granular column settlement is smaller than the vertical drain settlement by 40%. The columns have several advantages compared with pile and lime columns. Special equipment is necessary to construct lime columns, but conventional equipment can be used in stone column construction, which can be used in bored piles and vibro compactions.

They performed analytical calculations to estimate the geosynthetic tensile stiffness. Raithel et al. (2005) and Alexiew et al. (2005) introduced the successful use of the geosynthetic encased column. Rajagopal (2006) reported that the main advantages of the granular columns are to increase the bearing capacity, decrease the settlement, and accelerate the consolidation process. Wehr (2006b) concluded that a flexible footing has a better load-carrying capacity than a rigid footing due to the formation of wider shear zones near the footing edge and the additional shear zones between columns. Ambily & Gandhi (2007) investigated the behavior of stone columns using small-scale laboratory experiments and an axisymmetric FEA. The tests were performed on clay and sand in a cylindrical tank and

examine the influence of various design parameters. The findings indicate that the ultimate capacity of stone columns diminishes as column spacing increases and that the loss of ultimate capacity is negligible for columns spaced further than 3d apart. It is also observed that the ultimate column capacity increases with undrained shear strength, surcharge load, and the angle of internal friction of the stone backfill. Bulging was observed at a depth of 0.5 d when the column area alone was loaded, whereas no bulging was observed when the entire area was loaded. A group of researchers have explored various methods to increase the bearing capacity of footings. El Sawwaf and Nazir (2012) investigated unstable sand under the influence of simultaneous monotonic and cyclic loads. Fattah and Majeed (2012) reported that the use of stone cap above the stone column increases the bearing improvement ratio and decreases the settlement for all L/d ratios. The increase in stone cap thickness increases the bearing improvement ratio and decreases settlement for all L/d ratios. Replacement of the dense sand layer, and reinforcement using geogrid material were also investigated. The high material conductivity increases the consolidation rate and increases the subgrade stiffness (Azzam and Basha 2017). Mohamed et al. (2023) studied numerically the performance of strip footing supported by ordinary and encased stone.

It is proposed in this Paper to conduct a three-dimensional FEA using the PLAXIS 3D Foundation to examine the influence of various design parameters, such as diameter of stone columns, column length, and the number of columns, upon the settlement performance and deformational behavior of groups of stone columns. Effects due to oil contaminants are excessive settlement (Mackenzie, 1970); contaminants from oil exploration, transportation, production, and processing affect the safety of civil engineering structures (Preslo et al., 1989; Nicholson and Tsugawa, 1996; Shroff et al., 1998). SHIN, LEE, AND DAS 1999 with the decrease in the soil friction angle with oil-contaminated sand, the ultimate bearing capacity also decreases. When the oil content increases from zero to about 1.3%, the ultimate bearing capacity is reduced by about 75%. For 1.3%, the reduction in (qu) is not substantial. Villalobos (2007) made an experimental study on the bearing capacity of the foundation on various types of sand (Leighton Buzzard sand). The purpose of the investigation was to calculate the bearing capacity under a pure vertical load, and a series of tests were conducted with seven different skirt footings. The study was compared with the theoretical and experimental studies on the bearing capacity of shallow foundations in sand. Accordingly, it was concluded that the bearing capacity increased with the length of the skirts, which in some cases depends on the nature of the sand (internal angle of friction). The literature review shows that most studies have been conducted to determine the bearing capacity of footings located on soil slopes without any contamination effects. Nasr's (2015) study is one of the few studies examining the

bearing capacity of footings located on an oil-contaminated soil slope. The results of his experimental and numerical study were published with the aim of raising awareness of the behavior of strip footings located on sand slopes contaminated with benzene, light gas, petroleum, and heavy engine oil (Nasr 2015). In his study, the effect of contamination from zero to 4% of dry sand weight and the effect of changes in parameters, such as contaminated layer thickness.

Al-Obaidey and Shaia 2018 Two series of conventional laboratory tests were conducted to evaluate the increase in oil concentration on the geotechnical properties of fine and coarse soil samples at sites located within the Thi-Qar Governorate area. The study revealed that there is a major influence of crude and engine oil contamination on the engineering behavior of sandy soil. The following main conclusions can be drawn:

- . The increase in oil content causes a shift in the grain size distribution curve from finer to coarser ranges.
- . The liquid limit, plastic limit, and plasticity index increase significantly in the contaminated samples in comparison to non-contaminated samples.
- . The increase in oil content for sandy samples causes a reduction in shear stress because of the potential for soil inter-particle slippage, which would increase with increasing oil content and eventually decrease the shear strength of the soil.
- . The angle of internal friction of the sandy soil decreases upon pollution with petroleum products.

The soil may or may not be eligible for engineering construction projects, and it may need significant treatment. Therefore, it is required to have a better understanding of the general behavior and the corresponding geotechnical properties upon contamination. In Al-Adly et al. (2019), the results showed that the presence of oil in sand changes the mode of shear failure in sand under the footing from local shear failure to the punching shear failure.

There are limited studies on partially penetrating encased granular columns in contaminated sandy soils. The design of the encased and ordinary stone columns is still based on empirical methods without considering the contamination effect. Therefore, the present research attempts to realize and analyze the geotechnical response of stone columns that are installed in contaminated sand by studying the performance of strip footing supported by stone columns in contaminated sand. The research includes the study of contamination content. Oil contamination in soil, stemming from sources like oil tube leaks, product transportation, or excavation activities during oil operations, can induce significant changes in its physical, mechanical, chemical, and biological properties. Consequently, such soil may no longer meet the requirements for engineering construction projects and may necessitate substantial treatment measures. In regions associated with oil exploration and industry, such as the Thi-Qar Governorate in Iraq, fine and coarse

soils from a site at the University of Thi-Qar were intentionally contaminated with oil products ranging from 0% to 10% of their dry weight. Testing programs, including grading, Atterberg limit, vane shear, and direct shear tests, were conducted on the contaminated soil to assess its properties. The obtained results were then directly compared to those of the original uncontaminated soil to discern the variations induced by contamination.

The study's final outcomes highlighted the alterations in soil properties resulting from contamination; it is shown that by increasing the sand soil content of oil contamination, the angle of internal friction decreases. This relationship is the beginning of the geotechnical study of the current research on contaminated sand soil, and its impact is reinforced by ordinary stone columns (OSC) and encased stone columns (ESC), which have not been addressed in previous research.

I. NUMERICAL MODELLING NUMERICAL MODEL VERIFICATION

Numerical modeling plays a crucial role in analyzing geotechnical issues. Among the various techniques, finite element modeling (FEM) stands out. In this study, FEM, specifically implemented through "Plaxis 3D," was employed. This approach has been extensively discussed and utilized in prior research. The experimental results were juxtaposed with those derived from the simulated model in "Plaxis 3D." Advanced constitutive models were utilized to accurately simulate the behavior of contaminated sand, soil, and stone columns. Given that FEM involves approximation, several preliminary checks were conducted to ensure the accuracy of numerical analyses.

A. Verification using Nasr, 2015

In Nasr's (2015) study, the model geometry for the experimental setup is presented, alongside a view of the finite element mesh generated in the PLAXIS-3D model (see Figure 2). Triangular elements with 15 nodes were employed in the model. While the overall mesh size was medium, a finer mesh was defined around the working zone to reduce the number of elements in the analysis, thereby expediting the process.

The model featured sand slopes with dimensions of 550 mm in height and 800 mm in length, inclined at slope angles (β) of 26.60° (2H:1V) from the upper surface. The groundwater table was situated at a depth of 0.55 meters below the surface, with a depth of 300 mm. Additionally, the model incorporated two soil layers.

The Mohr-Coulomb model, representing the friction angle of granular soil, significantly influences a foundation's bearing capacity. To assess the impact of oil type and percentage on the angle of shearing resistance of sand (ϕ), multiple direct shear tests (conducted as per ASTM D3080 (ASTM, 2010b)) were performed on both clean and oil-contaminated sands, as depicted

ed in Figure 3. Strong correlations were observed between the obtained results and those reported by Nasr (2015).

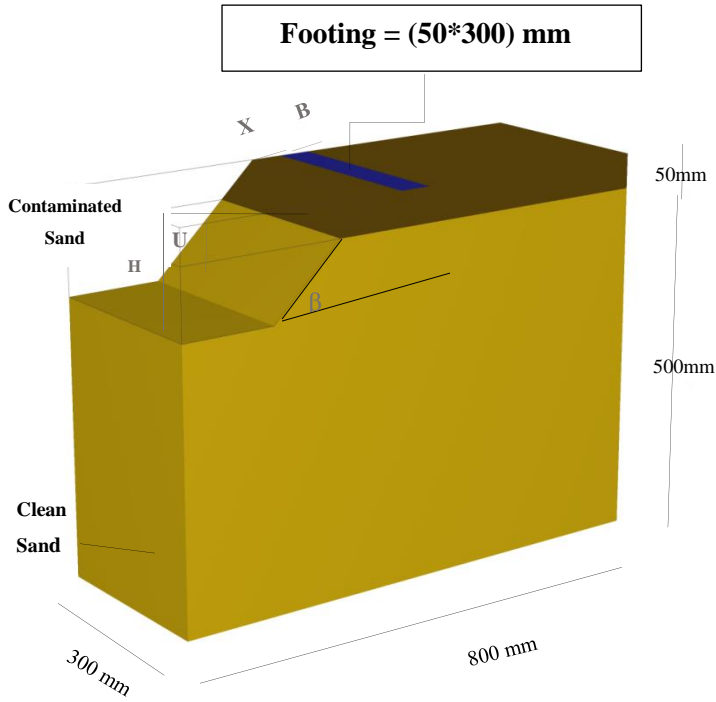


Figure 1. 3D Model geometry

Details about the experimental work referred to in Figure 1:

- 1-Constants: ($H = 150 \text{ mm}$, $B = 50 \text{ mm}$, $Dr = 53\%$, $\beta = 26.60^\circ$)
- 2-Footing location: ($X/B = 1.0$)
- 3-Thickness of contaminated layer: ($U/B = 1.0$)
- 4-Type of oil: (light oil)
- 5-Percentage of oil: (Oil content = 3%)
- 6-Slope: (2H:1V)

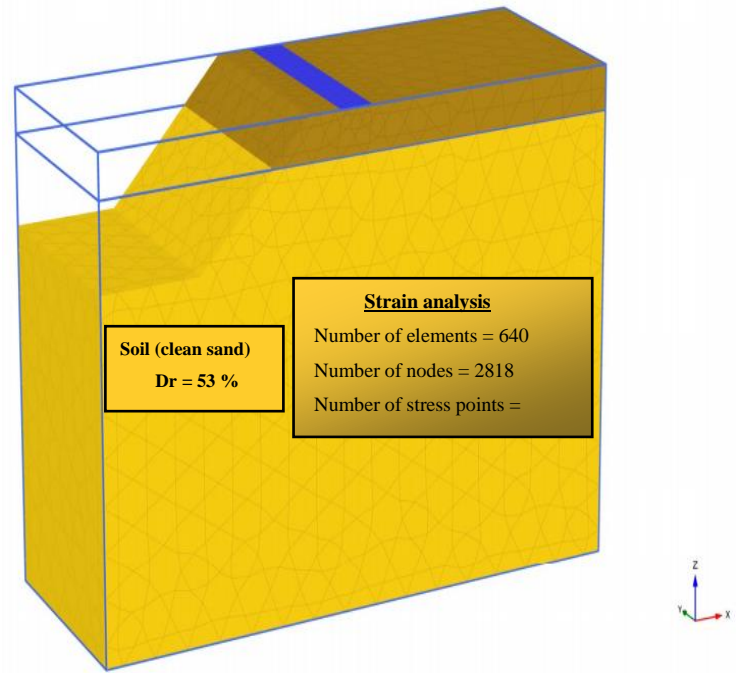


Figure 2: 3D Model geometry and mesh generation

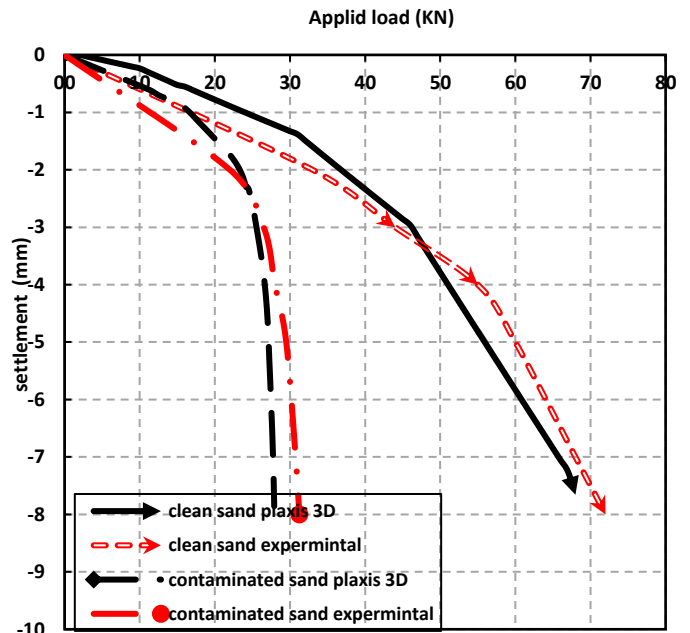


Figure 3. Validation of the results footing stress-settlement curves from PLAXIS 3D simulations on clean and contaminated sand slopes at ($U/B=1$, $X/B=1$ -with contaminated 3% oil) for Nasr, 2015.

The experimental study performed by Nasr, 2015 was used to validate the model as shown in "Figures 1," and "2,". "Figure 3" shows that the results were quite close between the model and the results of Nasr, 2015.

B. Verification using (Brinkgreve & Broere, 2006)

"Figure 4" depicts the geometric arrangement of the experimental model, while "Figure 5" illustrates the finite element mesh generated in the PLAXIS-3D model. The mesh comprised 15-node triangular elements. A medium-sized mesh was employed for the model, with a locally refined mesh around the working zone to optimize computational efficiency by reducing the number of elements.

The model's geometry included four encased sand columns, each with a diameter of 50mm and spaced 125mm apart, with the tip of the encased sand columns situated 620mm below the surface. The groundwater table depth was 0.02 meters beneath the surface. The model dimensions measured 1m in depth, 0.72m in breadth, and 2m in length.

The model consisted of three soil layers, with each layer's soil characteristics detailed in a table. The Hardening Soil model was employed, and the reference secant stiffness values from the CU tri-axial test were utilized to accurately represent the soil layers, as shown in "Figure 6". Notably, the findings of Brinkgreve and Broere (2006) exhibited a strong correlation with the results obtained in this study.

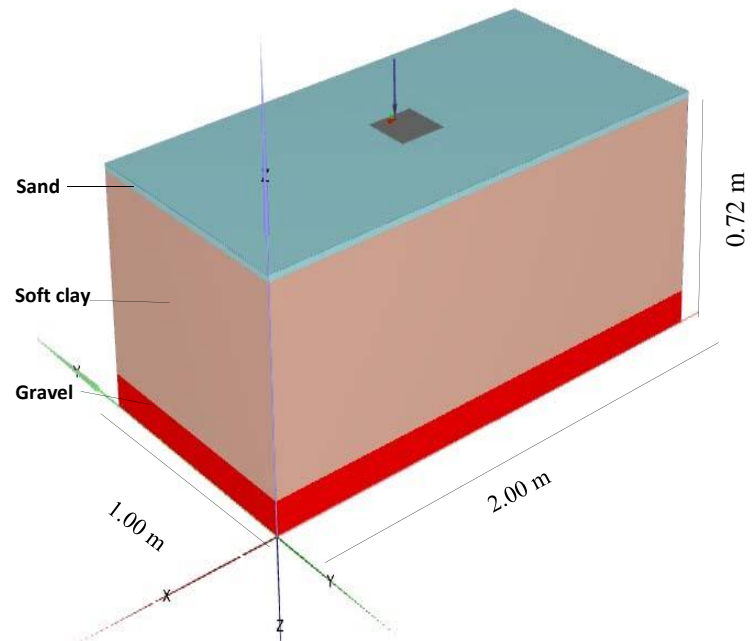


Figure 4. 3D Model geometry

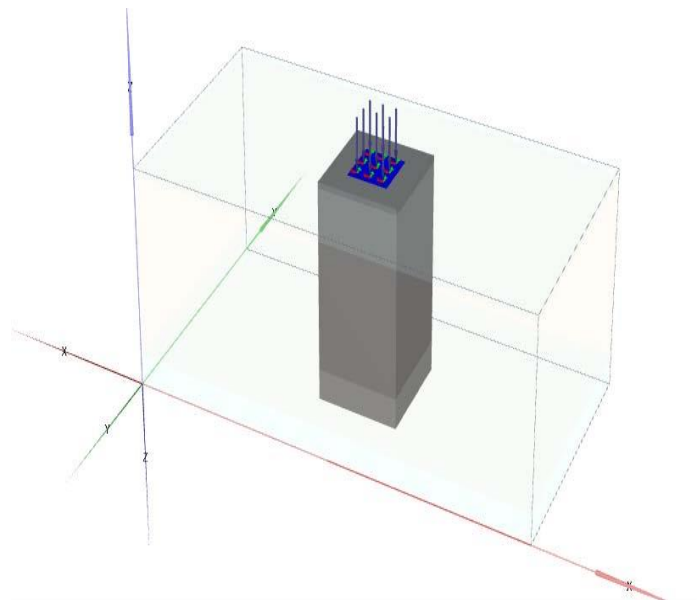


Figure 5. 3D Model geometry local mesh

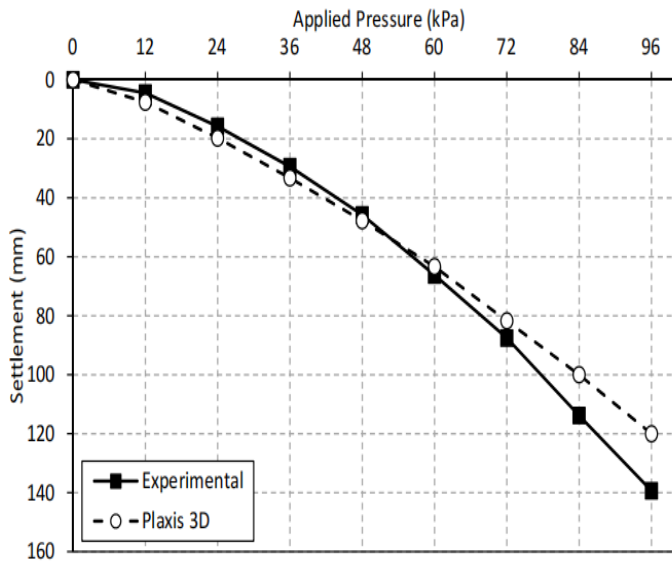


Figure 6. Validation of the load settlement curve results using ESC (L/H=0.6) for Brinkgreve & Broere (2006) utilizing the PLAXIS 3D program.

II. Numerical Model

The Finite Element Method (FEM) stands as an indispensable tool for tackling intricate engineering dilemmas, propelled by advancements in computer technology, which have catalyzed the proliferation of specialized software applications addressing diverse engineering challenges. Consequently, proficiency in mathematical modeling has become prerequisite for engineering education.

Among these solutions, PLAXIS-3D emerges as a prominent three-dimensional finite element (FE) software tailored for geotechnical applications. It simulates the behavior of soil and stone through intricate elemental models, setting a standard for theoretical geotechnical finite element analysis software, pioneered by researchers at Delft University of Technology.

PLAXIS facilitates computation of various geotechnical parameters, such as deformation, excess pore water pressure, and consolidation settlement, particularly excelling in handling nonlinear material behavior. Its wide-ranging applications encompass the investigation of contaminated and clean sand soil, notably in scenarios involving conventional and encapsulated stone columns.

In this study, PLAXIS 3D version 2.1 (2021) was utilized to inspect the structural components within the soil domain. The investigation focuses on a 3.00 m thick layer of polluted sand soil overlaying a clean sand layer 17.00 m deep, supported by multiple stone columns. To accommodate lateral effects, the domain width is set to 20.00 meters. Numerical modeling captures the behavior of strip footings on sand soil reinforced with stone columns. The sand soil is characterized by the Mohr-Coulomb model at rest, while plate attributes are defined for the strip footing. The strip footing measures 1.50 meters in width, 0.60 meters in thickness, with $EA = 2.1 \times 10^7$ kN/m and $EI = 2.29166 \times 10^5$ kN/m³, weighing 12.5 kN/m², and possessing Poisson's ratio $\nu = 0.2$.

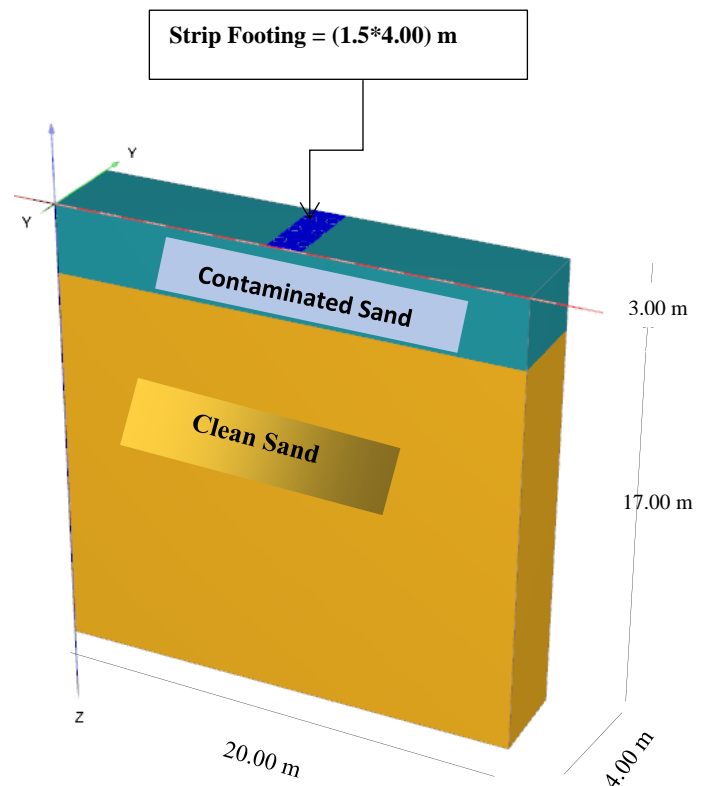


Figure 7. 3D Model geometry without stone column

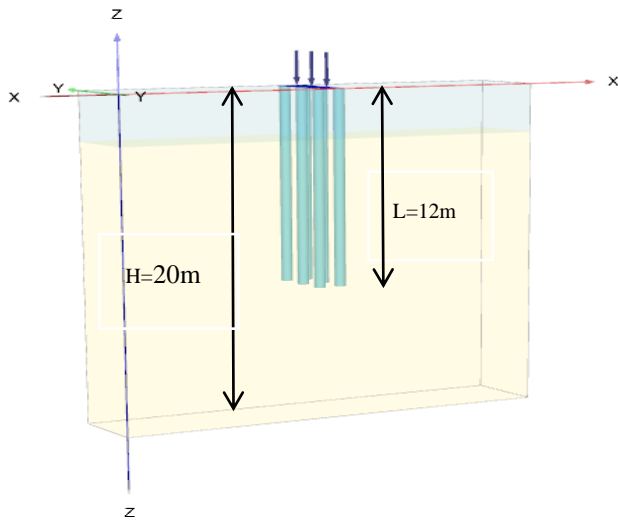


Figure 8. 3D Model geometry of (OSC)

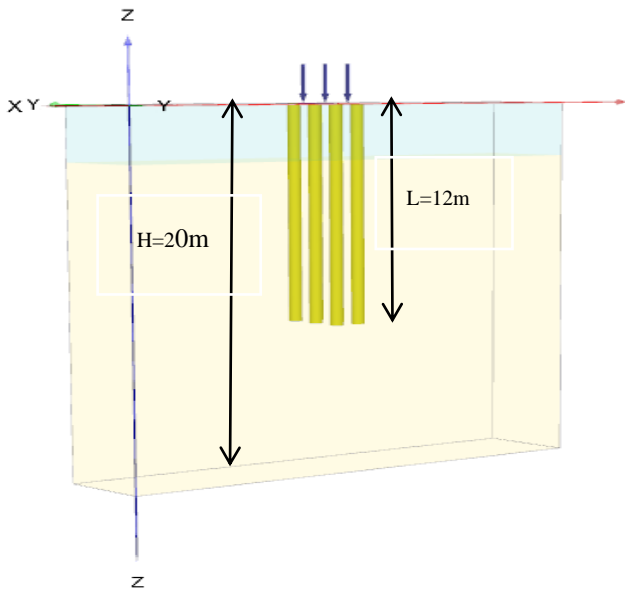


Figure 9. 3D Model geometry of (ESC)

3." In contrast, a linear elastic material model was adopted for modeling the footing, as indicated in "Table 2."

The model geometry utilized in this experiment is illustrated in "Figure 7." Three-dimensional meshes were generated for the sand, regular stone, and fully encased columns, as shown in "Figures "8," and "9," respectively. These visual representations aid in comprehending the structural configurations considered in the analysis.

A. Materials Properties

"Table 1" presents the characteristics of the soil materials used in the model (Al-Obaidy & Shaia, 2019). "Table 2" provides the attributes of the geogrid materials employed in the model. "Table 3" depicts the properties of the model footings utilized.

Table 1. Soil Properties used in PLAXIS 3D) Al-Obaidy & Shaia.2019)

Parameter	clean sand (Medium)	Contaminated sand (oil) (2%-5%- 10%)	Stone column
Material type	Drained	Drained	Drained
Type of material behavior	Mohr Coulomb	Mohr Coulomb	Mohr Coulomb
Young's modulus, Eref: kN/m ²	18000	11000	34000 -28000- 20000
Poisson's ratio	0.3	0.3	0.2
Cohesion, C: KN/m ²	0.3	0.3	----
Friction angle, Ø: °	34	31° - 27° - 24°	35° - 40° - 45°
Dilatancy angle, ψ: °	-----	-----	5° - 10° - 15°
Unit weight, γ: KN/m ³	17.54	17.54	22.25
Interface reduction factor, R _{int}	0.65	0.65	0.7

In this study, the PLAXIS 3D program was employed for comprehensive analysis. Under undrained conditions, the sand soil was characterized as Mohr-Coulomb material, with the Mohr-Coulomb technique utilized for modeling the stone column, as demonstrated in "Table 1." Additionally, a linear elastic geogrid model with variable stiffness characteristics was employed to simulate the Geogrid material, as depicted in "Table

Table 2. Footing Properties used in PLAXIS 3D (Nasr, 2015)

Parameter	Footing
Model type	Linear Elastic
Young's modulus, Es (kN/m ²)	21×10 ⁷
Poisson ' s ratio, v	0.20

Table 3. Geogrid Properties used in PLAXIS 3D (Tandel et al. 2013)

Parameter	Geogrid
Model Type	Linear Elastic
Axial stiffness, J (kN/m)	J ₁ = 500
	J ₂ = 1000
	J ₃ = 1500
	J ₄ = 2000
	J ₅ = 2500
Poisson's ratio, v	0.3

B. STUDIED SERIES AND PARAMETERS

A series of experiments were conducted to explore the effects of various parameters, including the internal friction angle of stone columns, on the durability of contaminated sandy soil. The investigations were conducted using both clean sand soil and sand soil contaminated with oil. Two types of stone columns were employed: ordinary stone columns (OSC) and encased stone columns (ESC).

The study considered the following parameters:

1. Height of contaminated sand (H contaminated), (H cont =3.00,4.00,5.00,6.00 and 7.00m)
2. Height of clean sand (H clean), (H clean =17.00, 16.00, 15.00, 14.00, and 13.00m)
3. Content of oil-contaminated sand, (cont oil =5% = $\phi^{\circ}=27^{\circ}$)
4. Number of stone columns (N), (N=6)

5. Diameter of stone columns (D), (D=0.50 and .60m)
6. Length of stone columns (L), (L= 12.00m)
7. Internal friction angle of stone column material (ϕ°), ($\phi^{\circ}=35^{\circ}$, 40° , and 45°)
8. Encasement Length, $L_{enc} / L = 1$ (fully encased)
9. Stiffness of encasement (J), (J = 500 to 2500)

C. Definition of the failure load

The double tangent approach is employed to determine the failure load, or ultimate bearing capacity (quilt). This method entails drawing two tangents on the pressure-settlement curve: one at the onset of the curve and another at its termination. These tangents are then extended backward until they intersect. The ultimate bearing capacity (quilt) corresponds to the load associated with this intersection point. The application of the double tangent approach for determining the ultimate bearing capacity is depicted in "Figure 10". This methodology provides a dependable means of evaluating the maximum load that the soil can withstand before failure occurs.

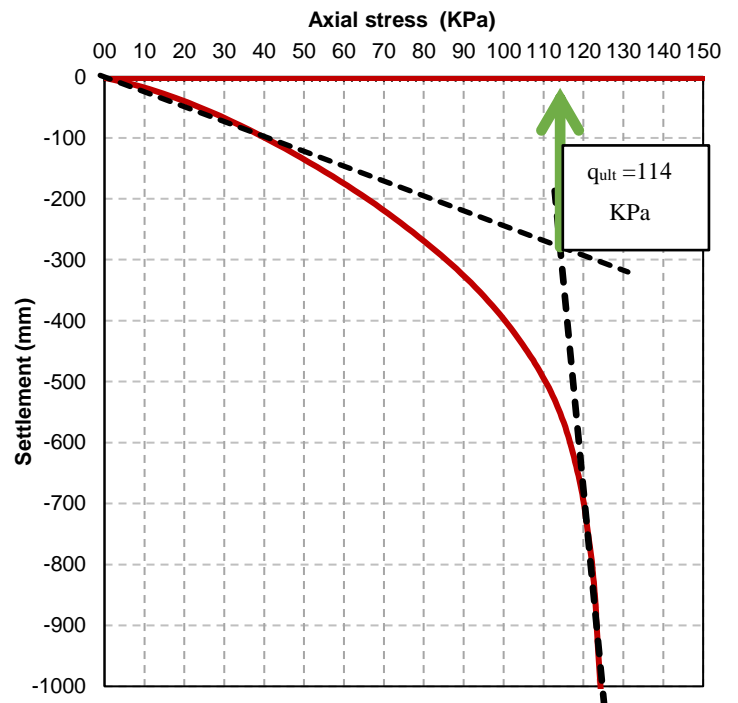


Figure 10. The pressure-settlement curve clarifies the double-tangent method

D. Bearing capacity ratio (BCR)

The investigation into the increase in bearing capacity employs the Bearing Capacity Ratio (BCR), a dimensionless quantity defined as the ratio of the final bearing capacities of soil improved with regular or encased stone columns to the final bearing capacities of clean sand soil without any improvement.

$$BCR = \frac{\text{The ultimate bearing capacity of improved soil}}{\text{The ultimate bearing capacity of unimproved soil}} \quad (1)$$

III. RESULTS AND ANALYSIS

A. The study aims to investigate how the friction angle (ϕ°) is influenced by the presence of oil contamination in sand, comparing its impact on oil-contaminated sand to that on clean sand.

A comprehensive understanding of the friction angle effect (ϕ°) on clean sand versus oil-contaminated sand necessitates meticulous examination. By scrutinizing this variable, valuable insights emerge regarding how variations in friction angle correlate with the presence or absence of oil pollution in the sand. This investigation yields crucial information about sand behavior under diverse conditions and its implications for workers' safety. Analysis of results from four distinct scenarios conducted using the Plaxis-3D program, wherein levels of oil pollution in sandy soil were systematically altered, reveals a discernible pattern. Specifically, a direct correlation emerges: higher degrees of oil pollution in sandy soil correspond to relative decreases in the soil's load-bearing capacity. Friction angle values (ϕ°) underwent adjustments to 24° , 27° , 31° , and 34° , respectively, with corresponding variations of 10%, 5%, and 2% in oil pollution levels, and solely clean sand conditions. Subsequently, the relationship between soil stress values for these four cases becomes apparent.

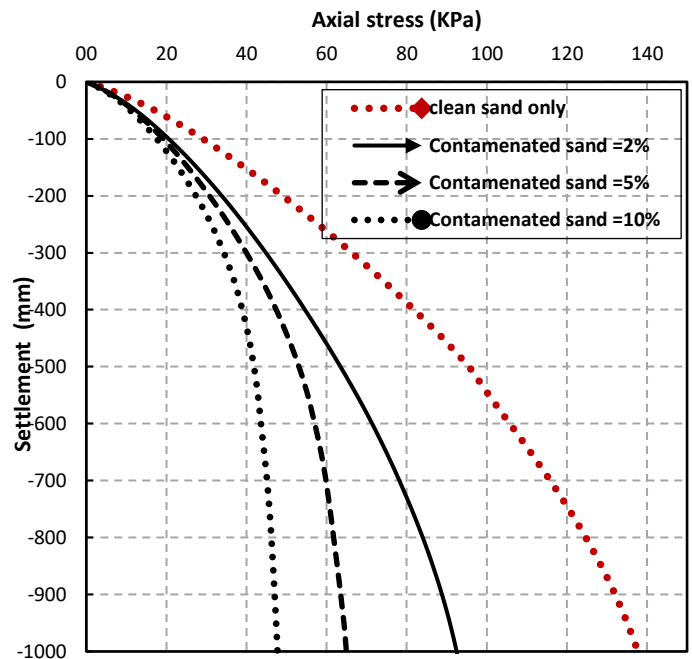


Figure 11. Relation between Axial stress and settlement at different oil-contaminated sand and clean sand at the variable friction angle

Triangular elements with 15 nodes were employed in the model. While the overall mesh size was medium, a finer mesh was defined around the working zone to reduce the number of elements in the analysis, thereby expediting the process.

B. Effect thickness of contaminated sand (T) at Content of oil-contaminated sand 5%

In this scenario, multiple models were analyzed using the PLAXIS-3D program. The models shared identical variable values, with the only difference being the thickness of the oil-contaminated sand soil. The investigated thickness values were 3.00, 4.00, 5.00, 6.00, and 7.00 meters, sequentially. Subsequently, the data were plotted to generate "Figure 12." The graphical depiction reveals a discernible trend: as the thickness of the oil-contaminated sand soil increases, the soil's capacity to support weight declines.

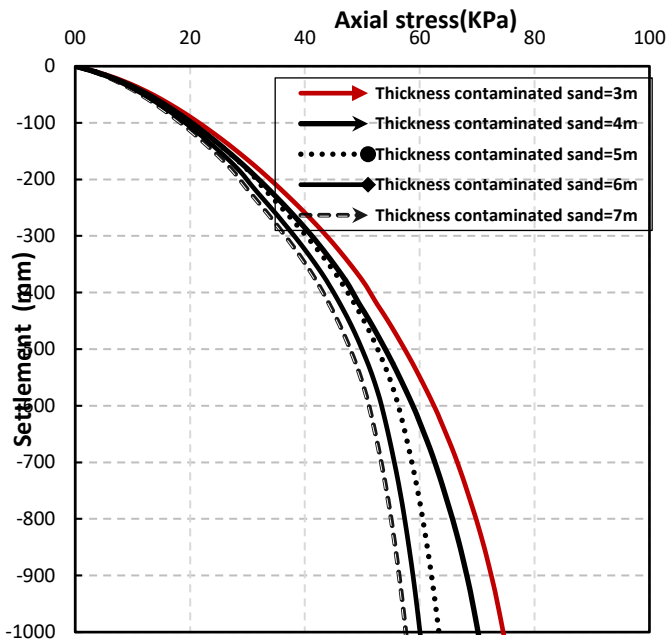


Figure 12. Axial stress – settlement curves for different thicknesses of contaminated sand at a Content of oil-contaminated sand 5%

The analysis of the data has revealed a notable finding regarding the internal angle of friction of contaminated sands, measured at 27 degrees. This conclusion finds support in the graphical representation provided in "Figure 12," which illustrates a distinct pattern. As depicted in the graph, the soil exhibits its maximum loading capacity at five specific points: 47 kN/m², 50 kN/m², 53 kN/m², 55 kN/m², and 58 kN/m². These points correspond to varying depths of the contaminated sand soil, namely 7m, 6m, 5m, 4m, and 3m, respectively.

This observation highlights the significant impact of pollution on the structural integrity of the soil, leading to a decrease in its load-bearing capacity as the depth of the oil-contaminated sand soil increases.

Table4. BCR for different thicknesses of oil-contaminated sand of (3-4-5-6-7m) and clean sand only

		thickness of contaminated sand (m)	q _{ult} KPa	BCR	BCR decrease
without SC	clean sand only		94		
	contaminated sand =2%	3	80	0.85	-15%
		4	76	0.81	-19%
		5	72	0.77	-23%
		6	67	0.71	-29%
		7	63	0.67	-33%

contaminated sand =5%	3	58	0.62	-38%
	4	55	0.59	-41%
	5	53	0.56	-44%
	6	50	0.53	-47%
	7	47	0.50	-50%
contaminated sand =10%	3	45	0.48	-52%
	4	43	0.46	-54%
	5	41	0.44	-56%
	6	39	0.41	-59%
	7	36	0.38	-62%

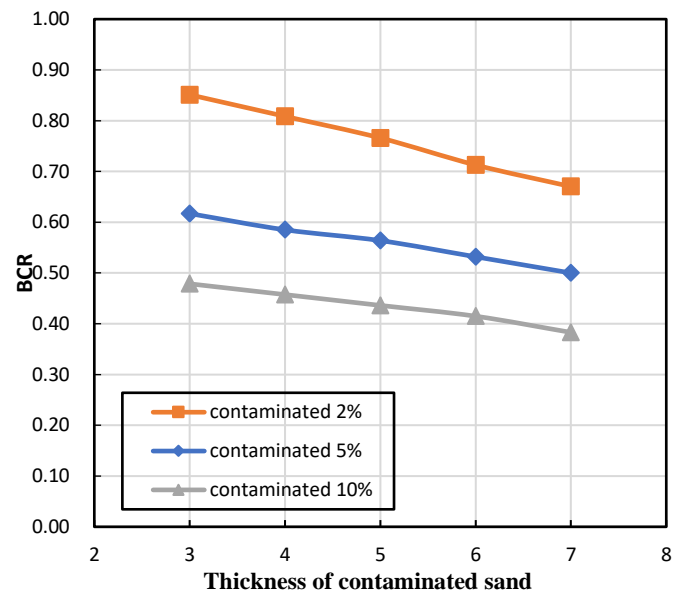


Figure 13. BCR for different thicknesses of oil-contaminated sand of (3-4-5-6-7)m and clean sand only

When analyzing oil-contaminated sandy soils at varying depths ranging from 3 meters to 7 meters, with contamination levels ranging from 2% to 10% compared to clean sandy soils, significant reductions in strength were observed, leading to diminished resilience of the contaminated soils. The contaminated sand soil exhibited a decrease in strength compared to clean sand soil, with reductions in endurance ratios of 0.85 times, 0.81 times, 0.77 times, 0.71 times, and 0.67 times for elevations at 3 m, 4 m, 5 m, 6 m, and 7 m, respectively, for a

contamination level of 2%. These reductions corresponded to decreases in Bearing Capacity Ratio (BCR) of 15%, 19%, 23%, 29%, and 33%, respectively. Similarly, for a contamination level of 5%, the contaminated sand soil showed reductions in endurance ratios of 0.62 times, 0.59 times, 0.56 times, 0.53 times, and 0.50 times for elevations at 3 m, 4 m, 5 m, 6 m, and 7 m, respectively. These reductions led to declines in BCR of 38%, 41%, 44%, 47%, and 50%, respectively. The most significant decreases in strength were observed for a contamination level of 10%, with reductions in endurance ratios of 0.48 times, 0.46 times, 0.44 times, 0.41 times, and 0.38 times for elevations at 3 m, 4 m, 5 m, 6 m, and 7 m, respectively. Correspondingly, these decreases resulted in declines in BCR of 52%, 54%, 56%, 59%, and 62%, respectively.

C. Effect of Internal Friction Angle (ϕ) and Diameter (D) of (OSC)

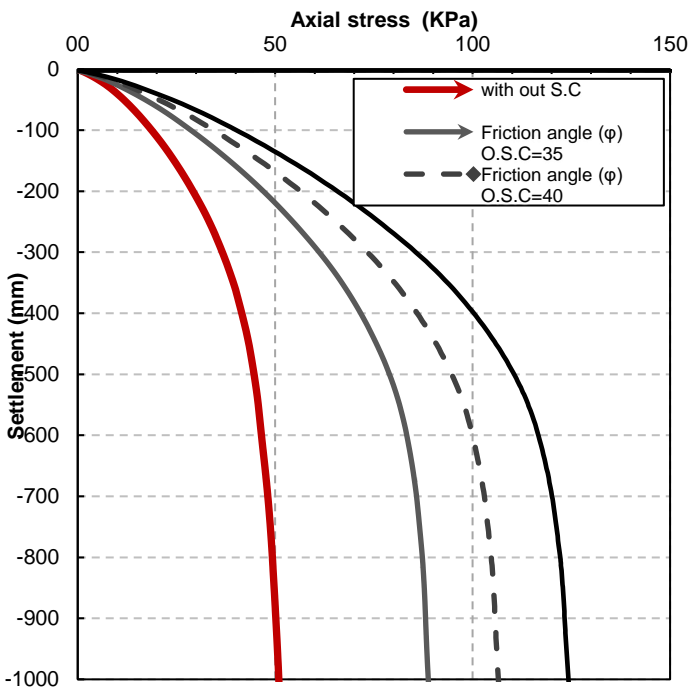


Figure 14. Axial stress - settlement curves for O.S.C (D=0.50 m, L=12.00 m) and without stone column at Content of oil-contaminated sand 5%

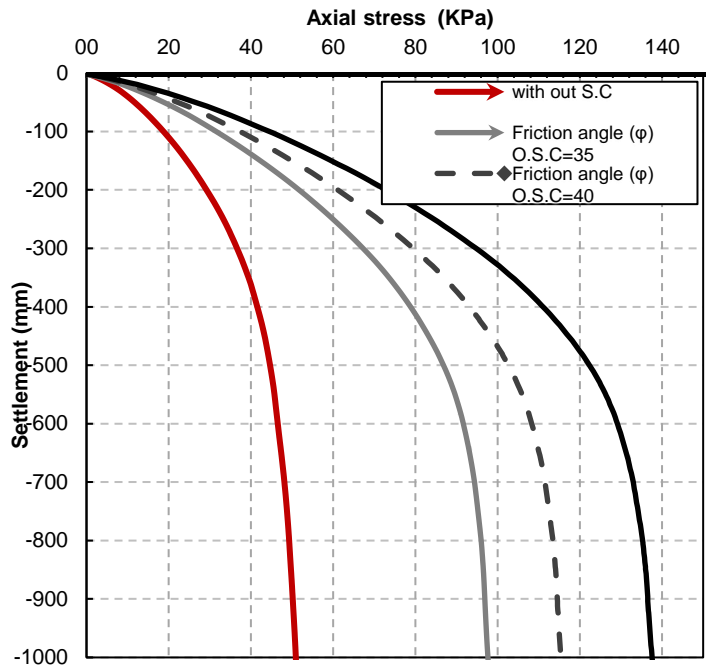


Figure 15. Axial stress - settlement curves for O.S.C (D=0.60 m, L=12.00 m) and without stone column at Content of oil-contaminated sand 5%

An investigation into the internal friction angle of conventional stone columns reveals a clear pattern: the soil's maximum load-bearing capacity increases to 80 kN/m², 90 kN/m², and 99 kN/m², respectively, as the angle rises from 35, 40, to 45 degrees. This correlation underscores the importance of higher internal friction angles in boosting soil stability, thereby enhancing its resistance to external forces. Elevating the friction angles of stone columns assumes a crucial role in optimizing soil performance, mitigating settlement, and bolstering load-bearing capacity, all essential for preventing structural issues. In Figure 14, it is evident that the soil's resilience significantly improves with the implementation of stone column reinforcement. The values double from 40 kN/m² without stone columns to 80 kN/m², 90 kN/m², and 99 kN/m² when utilizing standard 0.5-meter-diameter stone columns. Furthermore, as depicted in Figure 15, the results demonstrate further improvement when increasing the diameter of conventional stone columns to 0.6 meters. With internal friction angles of 35, 40, or 45 degrees, the soil's maximum load-bearing capacity increases to 92 kN/m², 98 kN/m², and 112 kN/m², respectively.

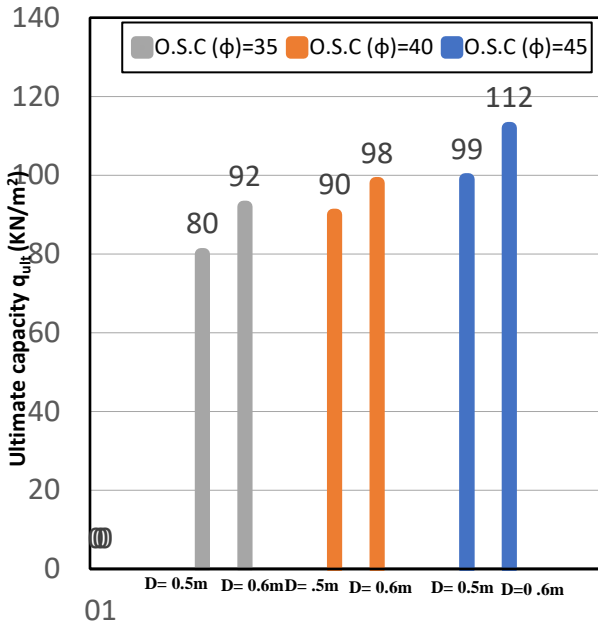


Figure 16. Ultimate bearing pressure for ordinary stone column (OSC) with different (ϕ) for stone column material

D. Effect of Stiffness of encasement (J) of (ESC)

Increased hardness of the body significantly impacts the endurance of enhanced stone walls. In this investigation regarding the influence of different geogrid reinforcements on the capacity to withstand stone column loads, various values were examined, denoted by $J = (500 \text{ kN/m}, 1000 \text{ kN/m}, 1500 \text{ kN/m}, 2000 \text{ kN/m}, \text{ and } 2500 \text{ kN/m})$. The study maintained stability with the following parameters:

- The stability ratio (L/D) was maintained at 24 for stone columns with a width of 0.5m and at 20 for columns with a width of 0.6m, where L represents the column length and D denotes the diameter of the stone column.
- The internal friction angle of the stone column material was kept constant at $\phi = 40^\circ$.
- The thickness of sand soil contaminated with used oils was set to 5m, while clean sand soil had a thickness of 15m in all cases.

The Axial Stress Adjustment Curve for Stone Column Behavior, illustrated in shapes 19-20, featured different values of stone column reinforcement hardness ranging from 500 kN/m to 2500 kN/m for diagonal diameters of 0.50 m and 0.60 m. The obtained results are consistent with U (2010) [27] and also align with the findings of Murugesan and Rajagopal (2006). The final loading capacity of encased stone columns with a diameter of 0.5m ranged from 190 KN/m² to 279 KN/m², while for a diameter of 0.6m, it ranged from 205 KN/m² to 310 KN/m², corresponding to varying levels of hardness.

Increasing the diameter of the stone column and its hardness both contributed to enhancing the soil's load-bearing capacity.

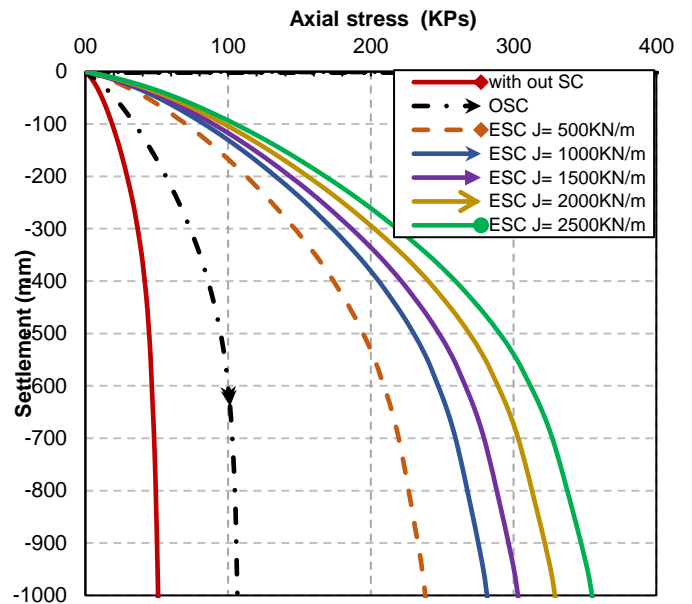


Figure 17 Axial stress-settlement curves for different (J) at (D=0.50 m, (ϕ) =40°)

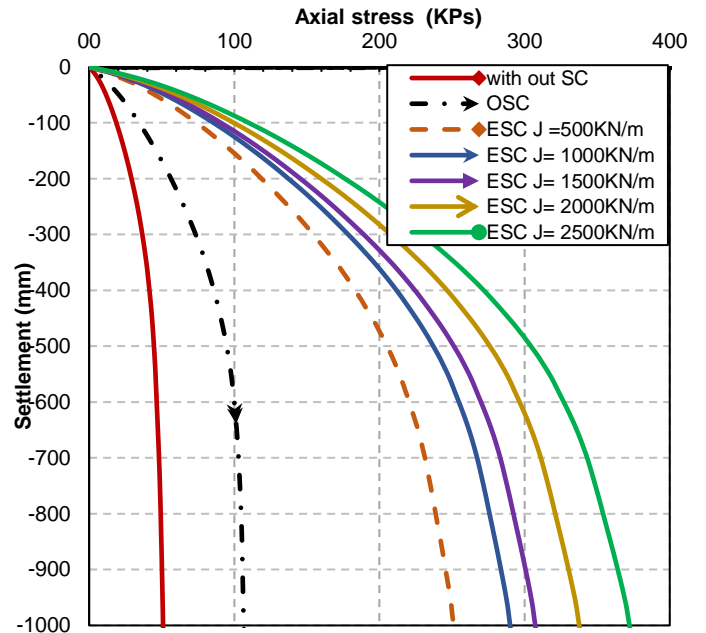


Figure 18 Axial stress-settlement curves for different (J) at (D=0.60 m, (ϕ) =40°)

Table 5. BCR for different (ϕ) values (D=0.50 m and 0.60 m), J =500 kN/m

		ϕ°	Q_{ult} (KPa)	BCR	BCR increase
D=0.5m	contaminated sand 5%		40		
	OSC	35	80	2	100%
		40	90	2.25	125%
		45	99	2.47	148%
	ESC	35	150	3.75	275%
		40	165	4.12	313%
45		178	4.45	345%	
D=0.6m	contaminated sand 5%		40		
	OSC	35	92	2.3	130%
		40	98	2.45	145%
		45	112	2.8	180%
	ESC	35	165	4.12	313%
		40	180	4.5	350%
45		190	4.75	375%	

tion angle of 45 degrees. This value increases to 180% for a diameter of $D = 0.60$ meters under the same internal friction angle. Similarly, for encased stone columns (ESC), the BCR increase reaches its maximum value at 345% for a diameter of $D = 0.50$ meters with an internal friction angle of 45 degrees. This value increases to 375% for a diameter of $D = 0.60$ meters at the same internal friction angle. SC with a diameter of $D = 0.50$ meters exhibited improvements in bearing capacity ratios on untreated soil, enhancing by approximately 2 times, 2.25 times, and 2.47 times for internal friction angles of 35 degrees, 40 degrees, and 45 degrees, respectively. Correspondingly, these improvements led to BCR increases on untreated soil by 100%, 125%, and 148%, respectively, for a diameter of 0.5 meters. For a diameter of 0.6 meters, BCR increased by 130%, 145%, and 180% for the same internal friction angles.

On the other hand, ESC demonstrated significantly higher improvements in bearing capacity ratios on untreated soil, enhancing by approximately 3.75 times, 4.125 times, and 4.45 times for internal friction angles of 35 degrees, 40 degrees, and 45 degrees, respectively. For ESC with a diameter of 0.5 meters, BCR improvements on untreated soil increased to 275%, 313%, and 345% for internal friction angles of 35 degrees, 40 degrees, and 45 degrees, respectively. The most notable enhancements were observed in the case of ESC with a diameter of 0.6 meters, where BCR improvements over untreated soil reached 4.125 times, 4.5 times, and 4.75 times for internal friction angles of 35 degrees, 40 degrees, and 45 degrees, respectively. Correspondingly, BCR improvements over untreated soil increased to 313%, 350%, and 375% for the same internal friction angles.

Table 6. BCR for different (ϕ°) values (D=0.50 m and 0.60 m), $J = 2500$

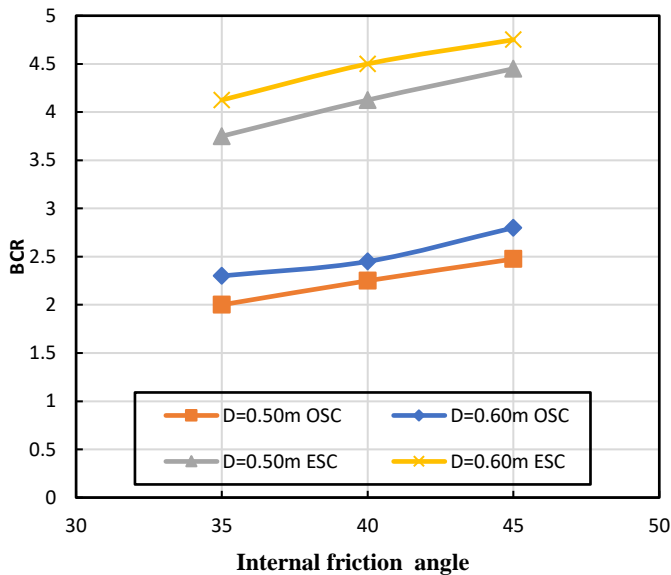


Figure 19. BCR for different (ϕ°), (D=0.50 m and D= 0.60 m of OSC and ESC)

For stone columns with a diameter (D) of 0.50 meters, it was observed that the Bearing Capacity Ratio (BCR) peaks at 148% for ordinary stone columns (OSC) with an internal friction

		ϕ°	Q_{ult} (KPa)	BCR	BCR increase
D=0.5m	contaminated sand 5%		40		
	OSC	35	78	1.95	95%
		40	83	2.07	108%
		45	95	2.37	138%
	ESC	35	260	6.5	550%
		40	290	7.25	625%
45		305	7.62	663%	
D=0.6m	contaminated sand 5%		40		
	OSC	35	90	2.25	125%
		40	95	2.37	138%

ESC	45	110	2.75	175%
	35	305	7.62	663%
	40	325	8.12	713%
	45	340	8.5	750%

625%, and 663% for internal friction angles of 35 degrees, 40 degrees, and 45 degrees, respectively. The most notable enhancements were observed in the case of ESC with a diameter of 0.6 meters, where BCR improvements over untreated soil reached approximately 7.625 times, 8.125 times, and 8.5 times for internal friction angles of 35 degrees, 40 degrees, and 45 degrees, respectively. Correspondingly, BCR improvements over untreated soil increased to 663%, 713%, and 750% for the same internal friction angles.

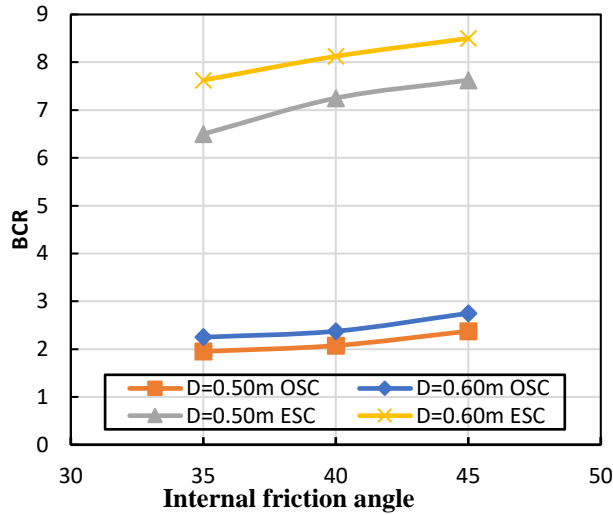


Figure 20. BCR for different (φ°), (D=0.40 m and D= 0.60 m of OSC and ESC)

For stone columns with a diameter (D) of 0.50 meters, it was observed that the maximum increase in the Bearing Capacity Ratio (BCR) was 138% for ordinary stone columns (OSC) with an internal friction angle of 45 degrees. This value increased to 175% for a diameter of D = 0.60 meters under the same internal friction angle. Similarly, for encased stone columns (ESC), the maximum BCR increase was 663% for a diameter of D = 0.50 meters with an internal friction angle of 45 degrees. This value increased to 750% for a diameter of D = 0.60 meters at the same internal friction angle.

OSC with a diameter of D = 0.50 meters exhibited improvements in bearing capacity ratios on untreated soil, with enhancements of approximately 1.95 times, 2.075 times, and 2.375 times for internal friction angles of 35 degrees, 40 degrees, and 45 degrees, respectively. Correspondingly, these enhancements led to BCR increases on untreated soil by 95%, 108%, and 138%, respectively, for a diameter of 0.5 meters. For a diameter of 0.6 meters, BCR increased by 125%, 138%, and 175% for the same internal friction angles.

In contrast, ESC showed significantly higher improvements in bearing capacity ratios on untreated soil, with enhancements of approximately 6.5 times, 7.25 times, and 7.625 times for internal friction angles of 35 degrees, 40 degrees, and 45 degrees, respectively. For ESC with a diameter of 0.5 meters, BCR improvements on untreated soil increased to 550%,

Table 7. BCR for different (J) values (D=0.50 m and 0.60 m), φ°=45

		J (kN/m)	q _u (KPa)	BCR	BCR in-crease
D=0.5 m	OSC		95	1	
	ESC	500	180	1.89	89%
		1000	238	2.5	151%
		1500	260	2.73	174%
		2000	278	2.92	193%
	2500	290	3.05	205%	
D=0.6 m	OSC		102	1	
	ESC	500	210	2.05	106%
		1000	280	2.74	175%
		1500	305	2.99	199%
		2000	325	3.18	219%
	2500	340	3.33	233%	

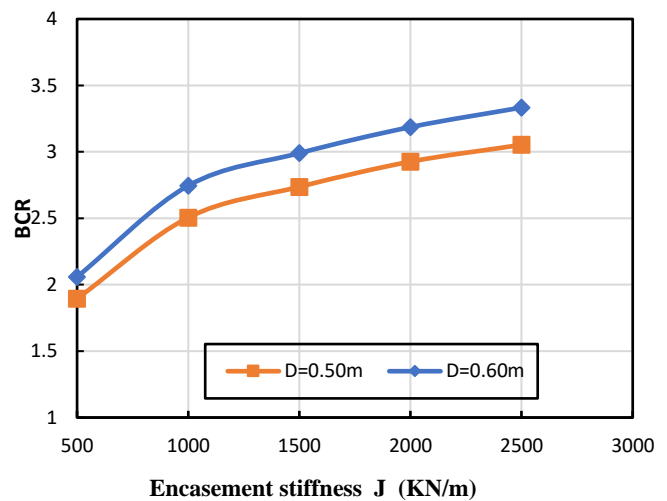


Figure 21. BCR for different (J), φ =45°

E. Effect of stone column material properties on lateral displacement

In this study, three values of the internal friction angle (φ = 35°, φ = 40°, and φ = 45°) were applied to stone columns with geogrid stiffness J = 1500 kN/m and full encasement (L-enc/L

= 1) to assess their impact on the performance of ordinary (OSC) encased stone columns against lateral deformation analysis. This analysis was conducted along a section line passing through the center of the stone column.

The lateral deformation (U_x) of an ordinary stone column (OSC) at the final stage was examined for various internal friction angles ($\phi = 35^\circ$, $\phi = 40^\circ$, and $\phi = 45^\circ$) with a diameter of $D = 0.50$ m. It was observed that the stone column primarily bulges in the upper section, approximately 1.5 times its diameter ($1.5D$), and diminishes with increasing depth, owing to reduced tension at deeper levels. Increasing the internal friction angle of stone columns was found to decrease the maximum lateral deformation. Compared to $\phi = 35^\circ$ (base case), the deformation of an ordinary stone column (OSC) decreases by 13% and 29%, respectively, when the internal friction angle is increased to $\phi = 40^\circ$ and $\phi = 45^\circ$. Table 9 illustrates this trend.

Table 9 also displays the maximum lateral distortion (U_x) of the encased stone column (ESC). In comparison to the deformation of a regular stone column with an angle of $\phi = 35^\circ$, the lateral deformation of the encased stone column improves by 62% (base case). Similarly, at angles of $\phi = 40^\circ$ and $\phi = 45^\circ$, the lateral deformation increases by 64% and 67%, respectively, for the encased stone column (ESC). Initially, when encasement commences, the stone column bulges to a length approximately three times its diameter ($3D$).

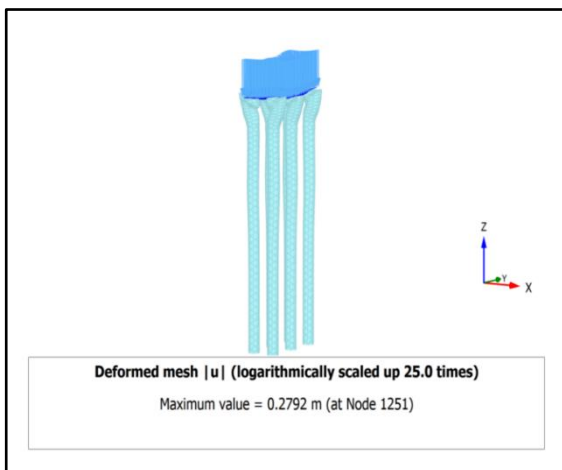


Figure 22. Mesh of (OSC), $D = 0.50$ m, for ($\phi=45$)

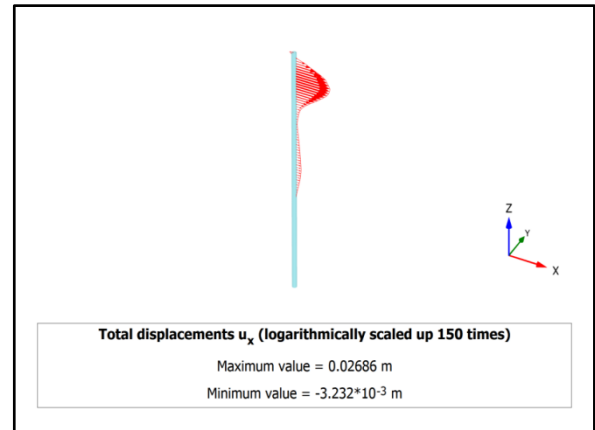


Figure 23. Total deformation of (OSC), $D = 0.50$ m, for ($\phi=45$) (Vertical section through the center of the stone column)

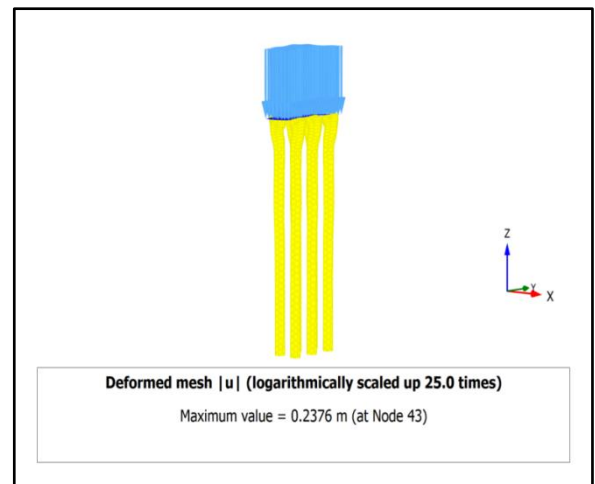


Figure 24. Mesh of (ESC), $D = 0.50$ m, for ($\phi=45$)

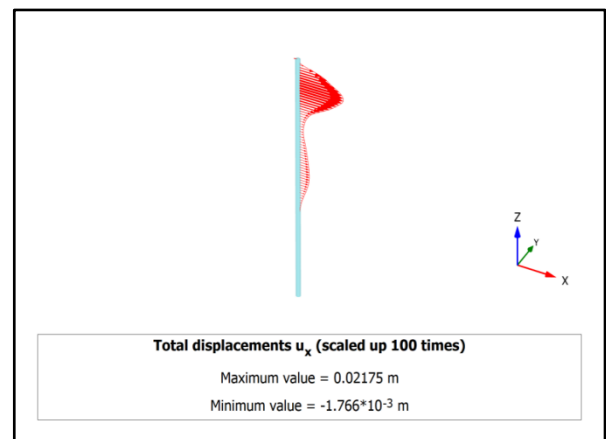


Figure 25. Total deformation of (ESC), $D = 0.50$ m, for ($\phi=45$) (Vertical section through the center of the stone column)

Table 8. Maximum lateral deformation different (ϕ°) values (D=0.50 m), J = 1500 kN/m

		ϕ°	qu(KPa)	Ux max(m)	Enhance (%)
D=0.5m	OSC	35	78	0.39	0% (Base case)
		40	83	0.32	17%
		45	95	0.27	30%
	ESC	35	240	0.23	41%
		40	260	0.19	51%
		45	290	0.17	56%

Table 9. Maximum lateral deformation different (J) values, (D=0.50 m), ($\phi^\circ=45$)

		J (kN/m)	qu(KPa)	Ux max(m)	Enhance (%)
D=0.5 m	OSC		95	0.27	0% (Bas case)
	ESC	500	180	0.25	7%
		1000	238	0.24	11%
		1500	260	0.23	15%
		2000	278	0.20	26%
		2500	290	0.18	33%

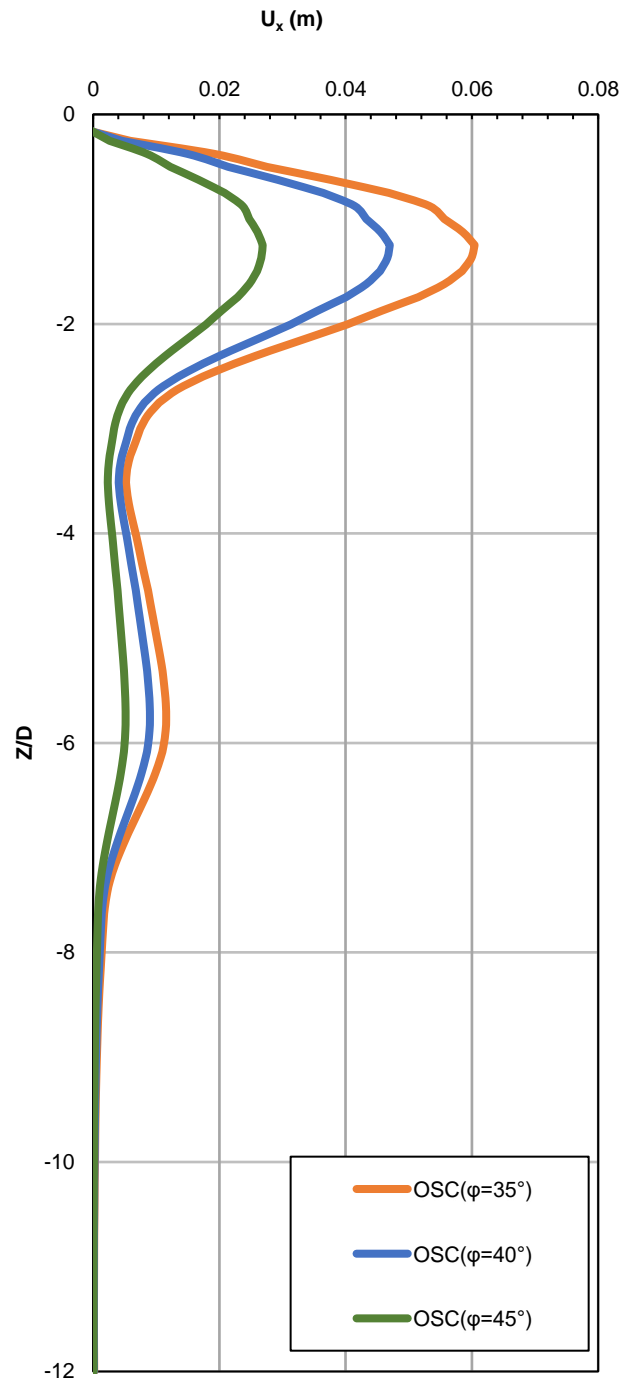


Figure 26. Lateral deformation (Ux) for ordinary stone column (OSC), D = 0.50 m, with different ($\phi^\circ= 35, 40, \text{ and } 45$)

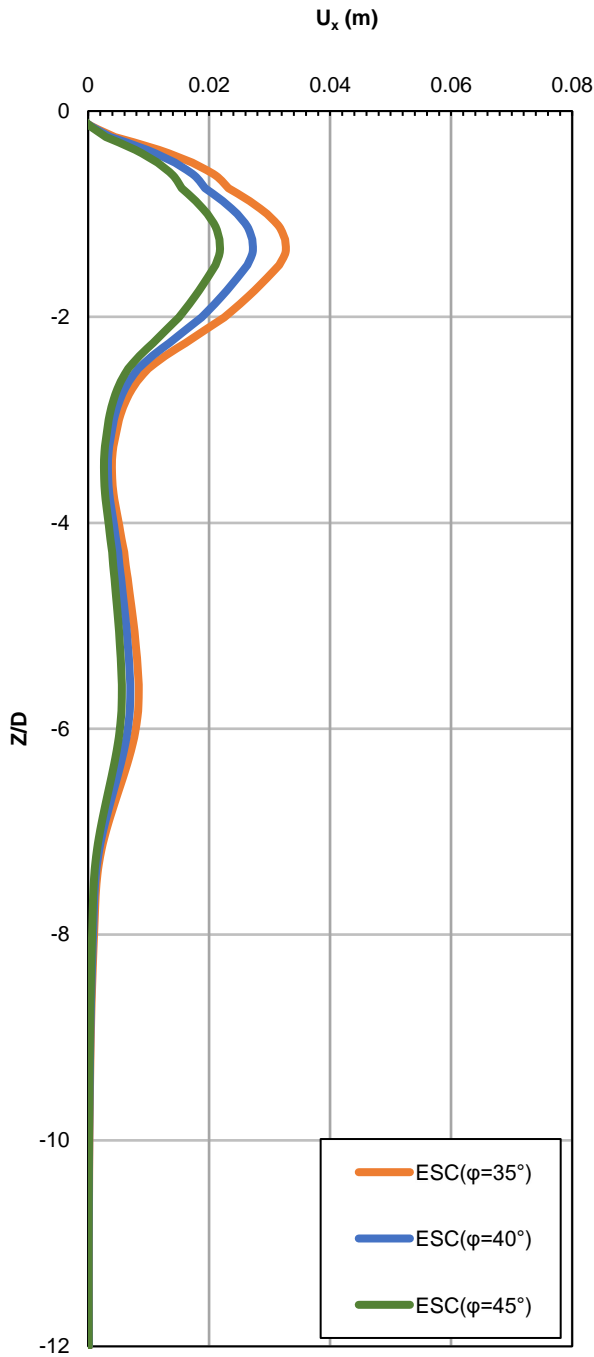


Figure 27. Lateral deformation (U_x) for encased stone column (ESC), $D = 0.50$ m, with different ($\phi = 35, 40,$ and 45)

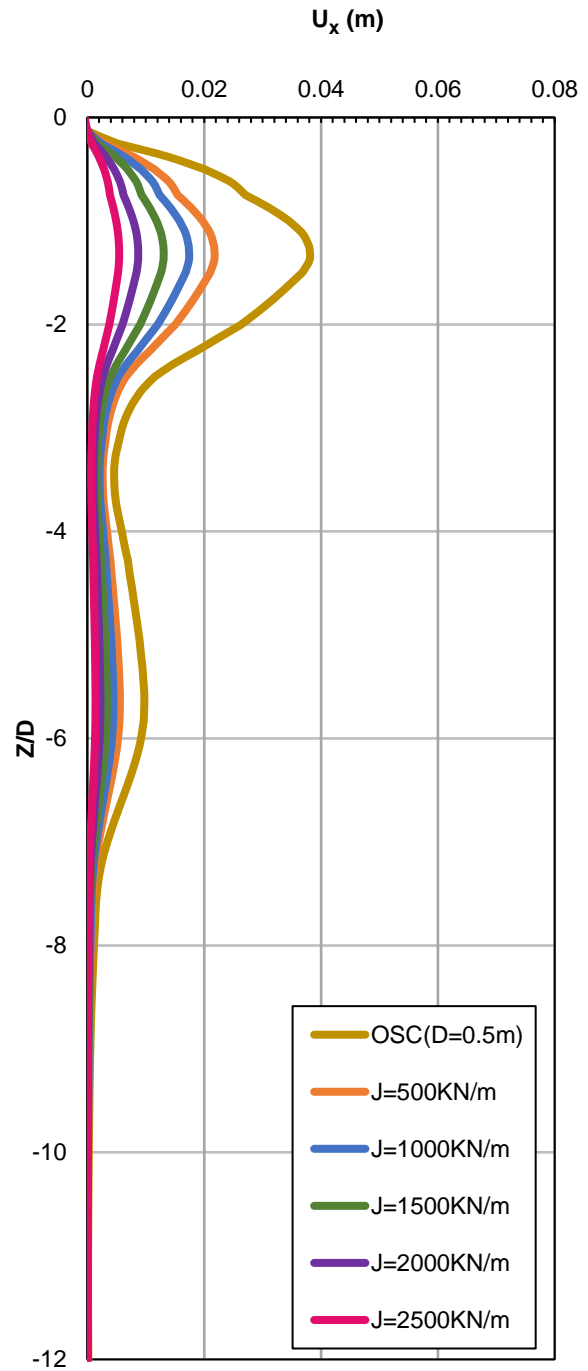


Figure 28. Lateral deformation (U_x) with different ($J = 500-1000-1500-2000$ and 2500), and OSC ($\phi = 45^\circ, D = 0.50$ m)

IV. Conclusions

This study investigated how various factors influenced the behavior of contaminated sand soil before and after reinforcement using encased stone columns (ESC) and ordinary stone columns (OSC). Several significant findings emerged from the analysis:

- At a 5% contamination level, the loading capacity increased by 23%, rising from 47 kN/m with a thickness of contaminated sand soil of 7 m to 58 kN/m with a thickness of contaminated sand soil of 3 m.
- In Ordinary Stone Columns (OSC), increasing the internal friction angle from 35° to 45° led to improved final tolerance and reduced settlement adjustment. Final tolerance increased by 95%, 108%, and 138% for internal friction angles of 35°, 40°, and 45°, respectively, compared to scenarios without stone columns. Settlement adjustment decreased by 125%, 138%, and 175% for stone column diameters of 0.5m and 0.6m, respectively.
- With an increase in the packaging coefficient's capacity from 500 kN/m to 2500 kN/m at an internal friction angle of 45°, the ultimate endurance and adjustment for ESC improved. Specifically, when the stone column's diameter was 0.5 meters, the percentages were higher than those of regular stone columns, ranging from 89% to 205%. For a diameter of 0.6 meters, the percentages ranged from 106% to 233% compared to standard stone columns.
- Ordinary stone columns provided greater benefits to column performance compared to contaminated sand without stone columns. Larger diameters were more advantageous, with the BCR increasing to 175% for a diameter of 0.6 m at an internal friction angle of 45°, compared to 138% for a diameter of 0.5 m.
- Encased stone columns outperformed contaminated sand without stone columns, with a 625% increase in BCR for a 0.5m diameter and a 663% increase for a 0.6m diameter, both at an internal friction angle of 40° and an encasement axial stiffness of 2500 kN/m.
- Settlement decreased with increasing encasement axial stiffness up to $J=1500$ kN/m, beyond which there was little variation in settlement values.
- Compared to regular stone columns, the bulging value of encased stone columns decreased by 80%. Bulging was observed in the upper portion of the encased stone columns, contrary to earlier findings where it typically occurred at the bottom, due to the impact of contaminated sandy soil.

References

- [1] PLAXIS-3D Version 2014 Manuals. "Finite Element Code for Soil and Rock Analysis". The Netherlands.
- [2] John Wiley & Sons (2015). "Principles and practice of ground improvement", the United States of America
- [3] Azzam, W., & Basha, A. (2018). Utilization of micro-piles for improving the sub-grade under the existing strip foundation: experimental and numerical study. *Innovative Infrastructure Solutions*, 3(1), 44.
- [4] Muzammil, S. P., Varghese, R. M., & Joseph, J. (2018). Numerical simulation of the response of geosynthetic encased stone columns under oil storage tank. *International Journal of Geosynthetics and Ground Engineering*, 4(1), 2–7.
- [5] Al-Obaidy, N., & Shaia, H. (2019). Evaluation of the Geotechnical properties of Oil-Polluted soil from two selected areas In Thi-Qar Governorate-Iraq. *University of Thi-Qar Journal*, 17–31.
- [6] Fattah MY, Shlash KT, & Al-Waily MJ. (2011) . Stress concentration ratio of model stone columns in soft clays. *Geotechnical Testing Journal*.;34(1):1.
- [7]Ahmed A. A.& Fattah M. Y.(2021).Distribution of Stresses Below Footings Supported by Stone Columns. *Journal of Engineering Science and Technology* .;16(2):1719-32.
- [8]Vahedian A, Mahini SS,& Aghdaei SA. (2014).A Short State-of-the-Art Review on Construction and Settlement of Soft Clay Soil Reinforced with Stone Column. *International Journal of Engineering and Technology*.
- [9] Vahedian, A., Mahini, S., & Aghdaei, S. A. (2014). A short state-of-the-art review on the construction and settlement of soft clay soil reinforced with stone columns. *International Journal of Engineering and Technology*, 6(5), 420–426.
- [10] Almeida, M., & Lima, B. (2014). Stone Columns Field Test: Monitoring Data and Numerical Analyses. *Geotechnical Engineering Journal of the SEAGS & AGSSEA*, 45(1), March 2014, ISSN 0046-5828.
- [11] Qassun, S. M. (2015). Analysis of embankment supported by stone columns encased with geosynthetic material. *International Journal of Civil Engineering and Technology*, 6, 97-107.
- [12] Muthukumar, M., & Sekar, S. K. (2015). Study on improving the performance of geosynthetic encased stone columns: numerical evaluation. *The International Daily Journal*, 40, 13-19.
- [13] Hamed, J., Abdolhosein, H., & Behrooz, M. (2012). Experimental and numerical investigation of the bearing capacity of adjacent footings on reinforced soil. *Electronic Journal of Geotechnical Engineering*, 17, 2597-2617.
- [14] Ali, M. (2019). Behavior of ordinary and encased stone columns end-bearing and floating in soft clay (numerical model). Springer, Cham.
- [15] Al-Aghbari, M. Y. (2007). Settlement of Shallow Circular Foundations with Structural Skirts Resting on Sand. *The Journal of Engineering Research*, 4(1), 11-1.
- [16] Joukar, A., & Boushehrian, A. H. (2020). Experimental Study of Strip Footings Rested on Kerosene Oil and Gas Oil Contaminated Sand Slopes. *Iranian Journal of Science and Technology, Transactions of Civil Engineering*, 44, 209–217.
- [17] Al-Adly , Fadhil , & Fattah. (2019).Bearing capacity of isolated square footing resting on contaminated sandy soil with crude oil.Egyptian Journal of Petroleum.
- [18] Fattah,M. , Majeed,G .(2012).A Study on the Behaviour of Geogrid Encased Capped Stone Columns by the Finite Element Method I.International Journal of GEOMATE.
- [19] Fattah,Y. , Majeed,G .(2012).Finite Element Analysis of Geogrid Encased Stone Columns .International Journal of GEOMATE,6 January 2012.
- [20]Al-Gharbawi AS,& Rajab NA.(2016). Comparison between sand columns and sand columns stabilized with lime or cement with stone columns embedded in soft soil. *Engineering and Technology Journal*.;34(15):2805-15.

- [21] Paul J., & Sindhu AR. (2018). Study on stress concentration ratio of stone column reinforced soft clay. *International Research Journal of Engineering and Technology (IRJET)*, 5(4):3535-9.
- [22] Sakr M, Shahin M, Farouk A, & Moneim K. (2017). Numerical Modeling of Stone Columns in Soft Clay for Drained and Undrained Conditions. *Electronic Journal of Geotechnical Engineering*, 22(6):1907-24.
- [23] Poon B, Chan K. (2013). Stress concentration ratio and design method for stone columns using 2D FEA with equivalent strips. In *Proceedings of the 18th International Conference on Soil Mechanics and Geotechnical Engineering* (pp. 2585- 2588).
- [24] Gaber M, Kasa A, Rahman NA, Alsharef JM. (2018). Comparison between unit cell and plane strain models of stone column ground improvement. *International Journal of Engineering & Technology*, 7(2):263-9.
- [25] Ambily, A. P., & Gandhi, S. R. (2007). Behavior of stone columns based on experimental and FEM analysis. *Journal of Geotechnical and Geoenvironmental Engineering*, 133(4), 405–415.
- [26] Ali, K., Shahu, J. T., & Sharma, K. G. (2014). Model tests on single and groups of stone columns with different geosynthetic reinforcement arrangements. *Geosynthetics International*, 21(2), 103-118.
- [27] Gniel, J., & Bouazza, A. (2010). Construction of geogrid encased stone columns: A new proposal based on laboratory testing. *Geotextiles and Geomembranes*, 28(1), 108–118.
- [28] Murugesan, S., & Rajagopal, K. (2007). Model tests on geosynthetic encased stone columns. *Geosynthetics International*, 14(6), 349–358.
- [29] Ghazavi, M., & Afshar, J. (2013). Bearing capacity of geosynthetic encased stone columns. *Geotextiles and Geomembranes*, 1–11. Doi:10.1016/j.geotexmem.2013.2013.04.003.
- [30] Shah, S. J., et al. (2003). Stabilization of fuel oil contaminated soil—A case study. *Geotechnical and Geological Engineering*, 21, 415–427.
- [31] Shin, Lee, & Das (1999). Bearing capacity of a model scale footing on crude oil-contaminated sand. *Geotechnical and Geological Engineering*, 17, 123–132.
- [32] Mohamed, M. K., Sakr, M. A., & Azzam, W. R. (2023). Geotechnical behavior of encased stone columns in soft clay soil. *Innovative Infrastructure Solutions*, 8, 80. doi:10.1007/s41062-023-01044-6.
- [33] Ali, M. (2018). Experimental and Numerical Modelling of Floating Encased Sand Columns Supporting Rigid Footings in Very Soft Clay (thesis). Cairo University, Egypt.
- [34] Al-Shammarie, H. A. (2013). An Experimental and Theoretical Study on Ordinary and Encased Stone Columns Underneath Embankment (Ph.D. Thesis). Civil Engineering Department, University of Baghdad, Iraq.
- [35] Abdulrasool, Ghaith. (2016). Effect of column stiffness on consolidation behavior of stone column-treated clay. Diss. University of Kansas.
- [36] Killeen, M. (2012). Numerical modeling of small groups of stone columns (thesis). National University of Ireland, Galway.
- [37] Al-Obaidy, N. (2017). Treatment of collapsible soil using encased stone columns (thesis). University of Birmingham Research Archive, Birmingham.
- [38] Ibrahim, M. (2018). Experimental and Numerical Modelling of Floating Encased Sand Columns Supporting Rigid Footings in Very Soft Clay. Retrieved from ResearchGate: <https://www.researchgate.net/publication/340827771>.
- [39] Rojas, C. (2016). Lucerne Train Station-Trial Shaft, a Case Study using HS-ss Model with Plaxis 3D. CORE. Retrieved from <https://core.ac.uk/display/81020832>.
- [40] Shien, N. G. (2013). Numerical study of floating stone columns. 123doc. Retrieved from <https://123docz.net/document/3049963>.
- [41] Tandel, Y. K., Solanki, C., & Desai, A. (2013). 3D FE Analysis of an embankment construction on GRSC and proposal of a design method. *International Scholarly Research Notices*, 2013, 1–11. doi:10.1155/2013/348973.
- [42] Al-Waily, M. J., & Al-Qaisi, M. S. (2023). Numerical Study of Stress Distribution in Soft Clay Treated with Stone Column. In *E3S Web of Conferences* (Vol. 427, p. 01006). EDP Sciences.